Acta Biomaterialia 45 (2016) 223–233

Contents lists available at ScienceDirect

Acta Biomaterialia

journal homepage: www.elsevier.com/locate/actabiomat

Full length article

Robust, active tumor-targeting and fast bioresponsive anticancer nanotherapeutics based on natural endogenous materials

Bingfeng Sun, Chao Deng *, Fenghua Meng, Jian Zhang, Zhiyuan Zhong *

Biomedical Polymers Laboratory, and Jiangsu Key Laboratory of Advanced Functional Polymer Design and Application, College of Chemistry, Chemical Engineering and Materials Science, Soochow University, Suzhou 215123, People's Republic of China

ARTICLE INFO

Article history:
Received 13 April 2016
Received in revised form 1 August 2016
Accepted 26 August 2016
Available online 27 August 2016

Keywords:
Nanomedicine
Hyaluronic acid
Polypeptide
Redox-responsive
Cancer therapy

ABSTRACT

The clinical success of cancer nanomedicines critically depends on availability of simple, safe and highly efficient nanocarriers. Here, we report that robust and multifunctional nanoparticles self-assembled from hyaluronic acid-g-poly(γ-benzyl-L-glutamate)-lipoic acid conjugates achieve a remarkably high loading (up to 25.8 wt.%) and active targeted delivery of doxorubicin (DOX) to human breast tumor xenograft *in vivo*. DOX-loaded nanoparticles following auto-crosslinking (DOX-CLNPs) are highly stable with little drug leakage under physiological conditions while quickly release ca. 92% DOX in 30 h under a cytoplasmic-mimicking reductive environment. The *in vitro* assays reveal that DOX-CLNPs possess a superior selectivity and antitumor activity to clinically used pegylated liposomal doxorubicin hydrochloride (DOX-LPs) in CD44 receptor overexpressing MCF-7 human breast cancer cells. Strikingly, DOX-CLNPs exhibit a superb tolerated dose of over 100 mg DOX equiv./kg, which is more than 5 times higher than DOX-LPs, and an extraordinary breast tumor accumulation of 8.6%ID/g in mice. The *in vivo* therapeutic studies in MCF-7 human breast tumor-bearing nude mice show that DOX-CLNPs effectively inhibit tumor growth, improve survival rate, and significantly decrease adverse effects as compared to DOX-LPs. DOX-CLNPs based on natural endogenous materials with high drug loading, great stability and CD44-targetability are highly promising for precision cancer chemotherapy.

Statement of Significance

We demonstrate that with rational design, simple and multifunctional anticancer nanotherapeutics can be developed to achieve highly efficient and targeted cancer chemotherapy. Doxorubicin-loaded multifunctional nanoparticles based on hyaluronic acid-g-poly(γ-benzyl-L-glutamate)-lipoic acid conjugates exhibit a high drug loading, superior stability, fast bioresponsivity, high tolerability, and obvious selectivity toward CD44-overexpressing tumors *in vivo*. These nanotherapeutics achieve effective tumor suppression, drastically improved survival rate and reduced side effects as compared to clinically used pegylated liposomal doxorubicin in MCF-7 human breast tumor-bearing nude mice. Unlike previously reported multifunctional nanomedicines, the present nanotherapeutics primarily based on natural endogenous materials are simple and straightforward to fabricate, which makes them potentially interesting for clinical translation.

1. Introduction

Nanomedicines present a most promising treatment for various cancers that are incurable nowadays [1,2]. It should be noted, however, that though significant scientific progress has been made in the past decade, few nanomedicines have been approved by the authorities for use in the clinics [3]. The clinical results reveal that current nanomedicines can indeed improve the pharmacokinetics and biodistribution of chemotherapeutic agents leading to a better tolerability and broader therapeutic window [3–6]. The therapeutic efficacy has, however, not much improved likely due to several existing challenges including drug leakage in circulation, poor tumor accumulation and cellular uptake, and inefficient drug release at the target site [7–9]. In order to achieve efficacious cancer treatments, a number of multifunctional nanocarriers have recently been developed and explored [10,11]. These studies

* Corresponding authors.
E-mail addresses: cdeng@suda.edu.cn (C. Deng), zyzhong@suda.edu.cn (Z. Zhong).

http://dx.doi.org/10.1016/j.actbio.2016.08.048
1742-7061/

provide a proof-of-concept that multifunctional nanomedicines through solving these systemic delivery barriers instigate better therapeutic outcomes in different tumor models [12–14]. Nevertheless, multifunctional nanocarriers that are typically made from novel and complex synthetic materials encounter involved preparation and potential safety concerns [10,15]. In addition, many reported multifunctional nanomedicines still suffer from a low drug loading level, poor stability, and insufficient tumor accumulation [9].

In this paper, we report robust, bioresponsive and highly specific anticancer nanotherapeutics based on fully natural endogenous materials i.e. hyaluronic acid (HA), L-glutamate and lipoic acid (LA) for high loading and targeted delivery of doxorubicin (DOX) to human breast tumor xenograft *in vivo* (Scheme 1). These multifunctional nanotherapeutics are readily assembled from hyaluronic acid-g-poly(γ-benzyl-L-glutamate)-lipoic acid (HA-PBLG-LA) graft copolymer. We recently reported that DOX-loaded reversibly crosslinked nanoparticles based on HA-LA conjugates (i.e. without PBLG block) exhibit potent antitumor effect toward CD44-positive drug-resistant human breast cancers *in vitro* and *in vivo* [16]. However, HA-LA nanoparticles revealed a moderate drug loading content (lower than 15.1 wt.%) and a relatively large particle size (154–225 nm). HA is a biocompatible and biodegradable natural polysaccharide, and has been approved by the FDA as intra-articular injection [17,18]. Notably, taking advantages of its effective targeting ability to CD44 receptor overexpressing cancer cells [16,19,20], HA-drug conjugates with paclitaxel, irinotecan, doxorubicin, and 5-fluorouracil have been developed and advanced to Phase I–III clinical trials for the treatment of various cancers such as bladder, colorectal, breast, lung, prostate, sarcoma [21]. PBLG as other polypeptides possesses excellent biocompatibility and biodegradability [22,23]. Notably, several nanomedicines based on polypeptides (NK105, NK012, NK911, NC-6004, NC-4016, NC-6300, CT-2103, CT-2106, etc.) have entered different phases of clinical trials [4,24–26]. Lipoic acid (LA) is a natural antioxidant produced by human body and has been employed to treat diseases like diabetes and Alzheimer's disease [27,28]. Remarkably, our results showed that the present multifunctional nanoparticulate doxorubicin possesses an ultrahigh drug loading level (up to 25.8 wt.%), small particle size (72–80 nm), superior stability, triggered cytoplasmic drug release, high tolerability and therapeutic index, and excellent tumor accumulation and selectivity toward CD44-overexpressing tumors *in vivo*, resulting in effective tumor suppression, drastically improved survival rate, and markedly decreased side effects as compared to clinically used pegylated liposomal doxorubicin hydrochloride (DOX-LPs) in MCF-7 human breast tumor-bearing nude mice.

2. Materials and methods

2.1. Materials

Unless stated otherwise, reactions were conducted in oven-dried glassware under an atmosphere of nitrogen using anhydrous solvents. Sodium hyaluronic acid (HA, molecular weight: 35 kDa, Shandong Freda Biopharm Co., Ltd.), lipoic acid (LA, 98%, J&K), N^{ε}-benzyloxycarbonyl-L-glutamic acid (H-Glu(OBzl)-OH, GL Biochem (Shanghai) Ltd.), 1,4-butanediamine (98%, J&K), N,N′-carbonyldiimidazole (CDI, 98%, J&K), 1-(3-dimethylaminopropyl)-3-ethylcarbodiimide hydrochloride (EDC, 98%, Alfa Aesar), N-hydroxysuccinimide (NHS, 98%, J&K), 1,4-dithio-D,L-threitol (DTT, 99%, Merck), glutathione (GSH, 99%, Roche), doxorubicin hydrochloride (DOX·HCl, >99%, Beijing Zhongshuo Pharmaceutical Technology Development Co., Ltd.), and doxorubicin hydrochloride pegylated liposome injection (DOX-LPs, 20 mg/mL, Shanghai Fudanzhangjiang Biomedical Co., Ltd) were used as received. N,N-dimethyl formamide (DMF) was dried by refluxing over anhydrous magnesium sulfate and distilled under reduced pressure before use. Dichloromethane (DCM), ethyl acetate, and petroleum ether (b.p. 60–90 °C) were refluxed over CaH_2 and distilled before use. All the other reagents and solvents were purchased from Sinopharm Chemical Reagent Co., Ltd. and used as received. BLG-NCA was prepared according to the Fuchs-Farthing method using triphosgene [29].

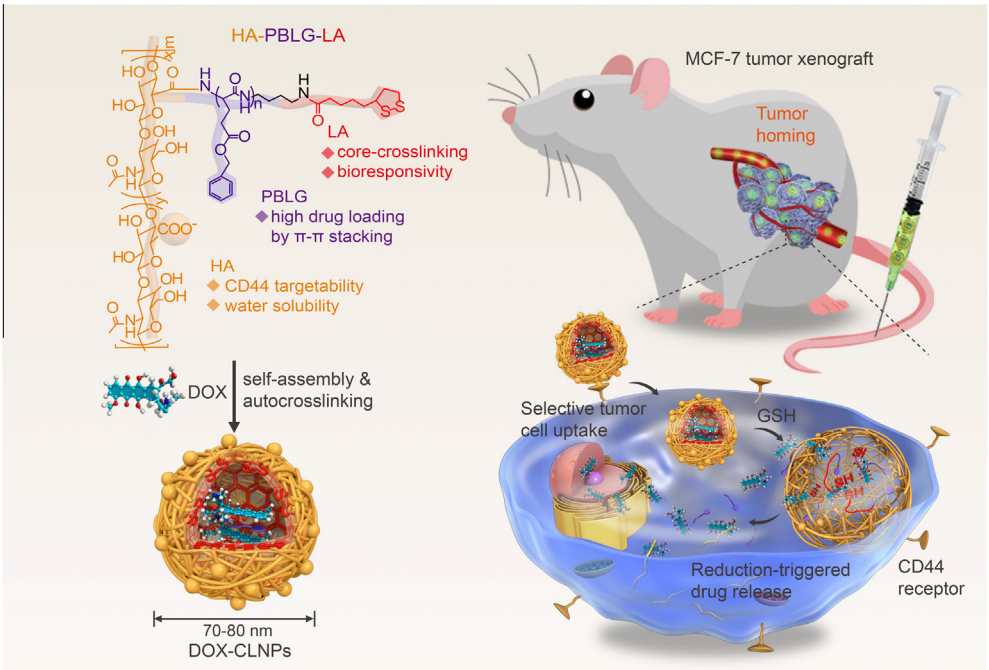

Scheme 1. Illustration of robust, active tumor-targeting and fast bioresponsive anticancer nanotherapeutics based on hyaluronic acid-g-poly(γ-benzyl-L-glutamate)-lipoic acid (HA-PBLG-LA) conjugates for high efficient and targeted breast tumor chemotherapy *in vivo*.

2.2. Characterization

^{1}H NMR spectra were recorded on a Unity Inova 400 spectrometer operating at 400 MHz using DMSO-d_6 or CF_3COOD as a solvent. The chemical shifts were calibrated against residue solvent signals. The size of nanoparticles was evaluated by dynamic light scattering (DLS). Measurements were carried out at 25 °C by a Zetasizer Nano-ZS from Malvern Instruments equipped with a 633 nm He–Ne laser using back-scattering detection. Zeta potential measurements were carried out using Zetasizer Nano-ZS instrument (Malvern) equipped with a standard capillary electrophoresis cell. Transmission electron microscopy (TEM) was carried out using a Tecnai G220 TEM operated at an accelerating voltage of 200 kV. The samples were prepared by dropping 20 μL of 0.5 mg/mL nanoparticles suspension on the copper grid followed by staining with 1 wt.% phosphotungstic acid.

2.3. Synthesis of N-lipoyl-1,4-butanediamine (LA-NH_2)

LA-NH_2 was prepared according to a previous report [30]. To a solution of LA (0.824 g, 4.0 mmol) in dry DCM (15 mL), a small excess of CDI (0.680 g, 4.2 mmol) was added over 5 min. This resulting solution was then added slowly to a stirred solution of 1,4-butanediamine (6 mL, 60 mmol). The reaction was allowed to proceed under magnetic stirring for 1 h at room temperature. The reaction mixture was extracted with NaCl aqueous solution (10 wt.%) and water for three times, dried by Na_2SO_4 at −24 °C overnight, and filtrated. The filtrate was concentrated via rotary evaporation and dried at room temperature in vacuo for 24 h. Yield: 93.3%. ^{1}H NMR (400 MHz, DMSO-d_6, Fig. S1, δ): 3.59 (m, methine of lipoic ring), 3.12 (m, –CONHC**H$_2$**–), 3.00 (t, –SSC**H$_2$**CH_2–), 2.53 (m, –C**H$_2$**NH_2), 2.40 and 1.85 (m, –$SSCH_2$C**H$_2$**–), 2.03 (t, –C**H$_2$**CONH–), 1.65 and 1.49 (m, –C**H$_2$**CH_2C**H$_2$**CH_2CONH–), 1.37–1.28 (m, –CH_2C**H$_2$**CH_2CH_2CONH–; m, –C**H$_2$**C**H$_2$**CH_2NH_2). The integral ratio of signals at δ 3.12 (–CONHC**H$_2$**–) and δ 3.59 (methine proton of lipoic ring) was close to 2, indicating that LA-NH_2 has been prepared successfully.

2.4. Synthesis of LA-PBLG polypeptides

LA-PBLG polypeptides were synthesized via the ring-opening polymerization of BLG-NCA using LA-NH_2 as an initiator. Briefly, a solution of LA-NH_2 (110.4 mg, 0.40 mmol) in dry DMF (10 mL) was rapidly added to a solution of BLG-NCA (1052.0 mg, 4.0 mmol) in dry DMF (10 mL) via syringe under a nitrogen atmosphere. The reaction was stirred at 30 °C for 3 days. The product was precipitated in excess diethyl ether, collected by centrifugation, and then dried in vacuo for 24 h. Yield: 92%. ^{1}H NMR (400 MHz, CF_3COOD, Fig. 1A, δ): 7.17 (s, –C_6**H$_5$**), 5.12 (s, –C**H$_2$**C_6H_5), 4.60 (m, –NHCOC**H**–), 4.36 (m, methine of lipoic ring), 3.44 (m, –CH_2 CONHC**H$_2$**–), 3.26 (t, –SSC**H$_2$**CH_2–), 2.58 (m, –$CH_2CONHCH_2CH_2$ CH_2C**H$_2$**–), 2.38 (t, –CH_2C**H$_2$**COO–), 2.10–1.89 (m, –C**H$_2$**CH_2COO–; t, –C**H$_2$**CONHCH_2–), 1.60–1.20 (m, –$SSCH_2$C**H$_2$**–; –C**H$_2$**C**H$_2$**C**H$_2$**CH_2 $CONHCH_2$C**H$_2$**C**H$_2$**CH_2–). The degree of polymerization (DP) of PBLG was determined to be 10.0 (denoted accordingly as $PBLG_{10}$) by comparing the integrals of signals at δ 7.17 and 3.26, which were assignable to the phenyl protons of PBLG and methylene protons of LA-NH_2, respectively. Similarly, $PBLG_{7.9}$ and $PBLG_{13.9}$ were prepared at BLG-NCA/LA-NH_2 molar feed ratios of 8 and 14, respectively.

2.5. Synthesis of HA-PBLG-LA conjugates

HA-PBLG-LA was obtained in two steps. Firstly, EDC (57.60 mg, 0.30 mmol) and NHS (17.25 mg, 0.15 mmol) were added to a stirred solution of HA (37.84 mg, 0.10 mmol –COOH) in D.I. water (3.0 mL), and then the pH of the solution was adjusted to 5.0 with 2 M HCl to preactivate the carboxyl groups of HA. After stirring for 0.5 h at room temperature, a certain amount of DMSO (40 mL) and a solution of LA-PBLG (122.80 mg, 0.05 mmol) in DMSO (6.0 mL) were added sequentially. The reaction was allowed to proceed at pH 9.0 for 24 h at 30 °C. The HA-PBLG-LA conjugate was isolated by extensive dialysis against DMSO for two days and deionized water for another two days (Spectra/Pore, MWCO 7000), and lyophilization. Yield: 78%. ^{1}H NMR (400 MHz, CF_3COOD, Fig. 1B, δ): HA: 4.20, 3.93–3.72 and 3.44–3.11; LA-PBLG: 7.17, 5.02, 4.60, 2.94, 2.85, 2.63, 2.39, 2.14–1.89, and 1.57–1.18. The degree of substitution (DS) was determined to be 14 by comparing the integrals of signals at δ 7.17 (phenyl protons of PBLG) and 4.20 (anomeric proton of HA).

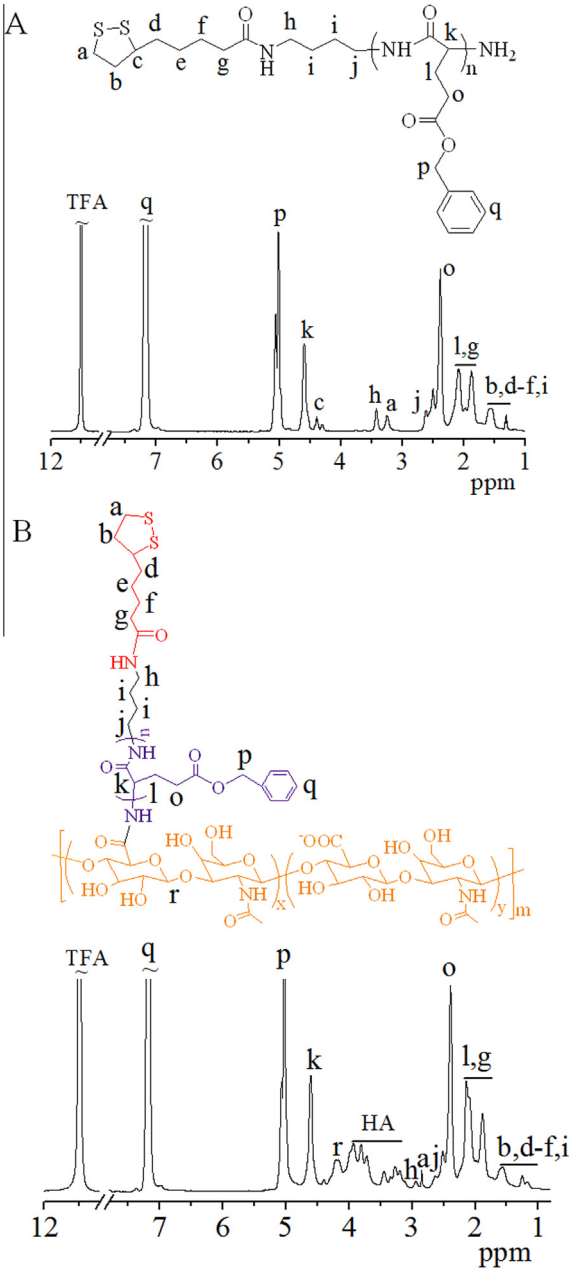

Fig. 1. ^{1}H NMR spectra (400 MHz, CF_3COOD) of (A) LA-$PBLG_{10}$ and (B) HA-PBLG-LA.

2.6. Preparation of crosslinked nanoparticles

HA-PBLG-LA noncrosslinked nanoparticles (NCLNPs) were prepared by dropwise addition of phosphate buffer (PB, pH 7.4, 10 mM) to a DMSO solution of HA-PBLG-LA under stirring at room temperature, followed by extensive dialysis against PB (pH 7.4, 10 mM) for 10 h using a dialysis bag (MWCO 3500 Da). The water was refreshed every one hour. The size and zeta potential of the noncrosslinked nanoparticles were measured by DLS. The critical micelle concentration (CMC) of NCLNPs was determined using pyrene as a fluorescence probe. The concentration of the conjugates varied from 4.88×10^{-5} to 0.2 mg/mL and the concentration of pyrene was fixed at 6×10^{-7} M. The fluorescence spectra were detected by FLS920 fluorescence spectrometer with the excitation wavelength at 330 nm, and the emission fluorescence at 373 and 383 nm. The CMC was estimated as the cross-point when extrapolating the intensity ratio I_{373}/I_{383} at low and high concentration regions.

Crosslinked HA-PBLG-LA nanoparticles (CLNPs) were obtained by the ring-opening polymerization of disulfide-containing lipoic ring using a catalytic amount of DTT under a nitrogen atmosphere, as reported previously [31,32]. Briefly, a DTT (2.6 μg, 10 mol% relative to the lipoyl units) solution in PB (13.0 μL) was added to 2.0 mL of HA-PBLG-LA nanoparticle dispersion (0.5 mg/mL). The mixture was stirred at room temperature under a nitrogen atmosphere for 24 h, and then dialyzed against PB (10 mM, pH 7.4) for 10 h (Spectra/Pore, MWCO 3500). The stability of CLNPs was evaluated via DLS following large volume dilution or incubation with 10% FBS. The reduction-sensitivity of CLNPs in the presence of 10 mM DTT solution was monitored by DLS measurement, following setting in a shaking bed at 200 rpm and 37 °C for a predetermined time.

2.7. Loading and reduction-triggered release of DOX

DOX loading into nanoparticle was accomplished by dropwise addition of PB (900 μL, 10 mM, pH 7.4) to a DMSO solution of HA-PBLG-LA (100 μL, 5 mg/mL) and DOX at DOX feed ratios of 20–40 wt.% under stirring at room temperature. The resulting drug-loaded nanoparticles were crosslinked as described above using a catalytic amount of DTT (10 mol% relative to the lipoyl units), followed by dialysis against PB (10 mM, pH 7.4) for 12 h (Spectra/Pore, MWCO 3500) to obtain DOX-loaded crosslinked nanoparticles (DOX-CLNPs). The dialysis medium was changed per hour, and the whole procedure was performed in the dark. For determination of drug loading content (DLC), the solution of DOX-CLNPs was diluted with DMF (30-fold) followed by sonification, and analyzed using fluorescence measurement (FLS920) with excitation at 480 nm and emission at 560 nm. Calibration curve of DOX fluorescence was obtained with different DOX concentrations in DMF solution. Drug loading content (DLC) and drug loading efficiency (DLE) were calculated according to the following formula:

$$\text{DLC (wt.\%)} = (\text{weight of loaded drug/total weight of polymer and loaded drug}) \times 100$$

$$\text{DLE (\%)} = (\text{weight of loaded drug/weight of drug in feed}) \times 100$$

The drug release of DOX-CLNPs was studied using a dialysis tube (Spectra/Pore, MWCO 12000) at a nanoparticle concentration of 0.2 mg/mL under shaking (200 rpm) at 37 °C in two different media: (i) PB (10 mM, pH 7.4), and (ii) PB (10 mM, pH 7.4) containing 10 mM GSH. Typically, 0.6 mL of DOX-loaded nanoparticle dispersion was dialyzed against 25 mL of the corresponding medium to acquire sink conditions. At desired time intervals, 5.0 mL of release medium was taken out and replenished with an equal volume of fresh medium. The amount of released DOX was determined by fluorescence measurement (FLS920). The release experiments were conducted in triplicate, and the results presented were the average data with standard deviations.

2.8. In vitro cytotoxicity assays

The cytotoxicity of HA-PBLG-LA CLNPs was evaluated in human breast cancer cells (MCF-7), which are known to express a high level of CD44 receptors [16]. The cells were plated in a 96-well plate (5000 cells/well) with 80 μL DMEM media supplemented with 10% fetal bovine serum, 1% L-glutamine, and antibiotics penicillin (100 IU/mL), and streptomycin (100 μg/mL) for 24 h. When the cells reached about 70% confluence, bare nanoparticles in 20 μL PB were added to yield final nanoparticle concentrations of 0.2, 0.4, 0.6, 0.8 and 1.0 mg/mL. The cells were cultured in an atmosphere containing 5% CO_2 at 37 °C for 48 h. Then, 3-(4,5-dimethyl thiazol-2-yl)-2,5-diphenyl tetrazoliumbromide (MTT) solution (10 μL, 5 mg/mL) in PBS was added to each well. After incubation for 4 h, the supernatant was carefully aspirated and 150 μL DMSO was added into each well to dissolve the formazan crystals generated by live cells for 10 min. The absorbance was measured at a wavelength of 570 nm using a microplate reader (Bio-Tek, ELX808IU). The cell viability (%) was determined by comparing the absorbance at 570 nm with control wells containing only cell culture medium. The experiments were performed in quartets. The antitumor activity of DOX-CLNPs and DOX-LPs was also examined by MTT assays in a similar way. The final DOX concentration in DOX-CLNPs or DOX-LPs incubated with MCF-7 cancer cells was fixed at 0.01, 0.1, 0.5, 1, 5, 10, 20 and 40 μg/mL. U87 cells that have been reported to express a low level of CD44 receptors [33,34] were used as a control. The inhibition experiments were performed by pretreating MCF-7 cells with free HA (5 mg/mL) for 4 h prior to incubating with DOX-CLNPs.

2.9. Flow cytometry assays and confocal microscopy measurements

Flow cytometry assays and confocal microscopy measurements were employed to investigate the cellular uptake and intracellular drug release behaviors of DOX-CLNPs in MCF-7 cells. The cells were cultured on microscope slides in a 6-well plate (1×10^6 cells/well) using DMEM media supplemented with 10% fetal bovine serum, 1% L-glutamine, and antibiotics penicillin (100 IU/mL), and streptomycin (100 μg/mL) for 24 h to reach 70% confluence. DOX-CLNPs or DOX-LPs in 200 μL PB were added to each well (10.0 μg DOX/mL). After incubation at 37 °C for 8 h, the cells were detached by 0.25% (w/v) trypsin and 0.03% (w/v) EDTA. The suspensions were centrifuged at 1000 rpm for 3 min, and the cells were collected following washing twice with PBS, and then re-suspended in 500 μL PBS. Fluorescence histograms were then recorded with a BD FACSCalibur flow cytometer (Becton Dickinson, USA) and analyzed using Cell Quest software. We analyzed 10,000 gated events to generate each histogram. The gate was arbitrarily set for the detection of FITC fluorescence. The inhibition experiments were performed by pre-treating MCF-7 cells with free HA (5 mg/mL) for 4 h prior to incubating with DOX-CLNPs.

The cellular uptake and intracellular drug release behaviors of DOX-CLNPs were also monitored using confocal laser scanning microscopy (CLSM). MCF-7 cells were cultured on microscope slides in a 24-well plate (2×10^4 cells/well) using 400 μL DMEM media containing 10% fetal bovine serum, 1% L-glutamine, and antibiotics penicillin (100 IU/mL) and streptomycin (100 μg/mL). After 24 h, DOX-CLNPs or DOX-LPs in 100 μL PB was added to each well (DOX dosage: 10.0 μg/mL), and incubated with cells for 8 h or 12 h. Then, the culture medium was removed and the cells on

microscope plates were washed three times with PBS, then fixed with 4% paraformaldehyde solution for 15 min and washed with PBS for three times. The cell nuclei were stained with 4′,6-diami dino-2-phenylindole (DAPI, blue) for 15 min and washed with PBS for three times. The fluorescence images were obtained using a confocal microscope (TCS SP5). The inhibition experiments were performed by pretreating MCF-7 cells with free HA (5 mg/mL) for 4 h prior to incubating with DOX-CLNPs.

2.10. Blood circulation

The mice were handled under protocols approved by Soochow University Laboratory Animal Center and the Animal Care and Use Committee of Soochow University. To measure the DOX level in blood in mice treated with DOX-CLNPs or DOX-LPs at a DOX concentration of 10 mg/kg, about 100 μL of blood was withdrawn from the orbit of Kunming (KM) mice at different time points, and dissolved in 0.1 mL of lysis buffer (1% Triton X-100) with brief sonification. DOX was extracted by incubating blood samples in 0.5 mL DMF containing 20 mM DTT overnight. After centrifugation at 23 krpm for 20 min, the DOX level of the supernatant was determined by fluorescence measurement. The blood circulation followed a typical two compartment model: a distribution phase with usually a rapid decline, and an elimination phase with usually a long period, which is the predominant process for drug clearance. The half-lives of two phases (t_1 and t_2) were calculated according to the following formula:

$$y = A_1 \times \exp(-x/t_1) + A_2 \times \exp(-x/t_2) + y_0$$

2.11. In vivo imaging and biodistribution

To monitor the nanoparticle distribution *in vivo*, fluorescent molecule DIR was loaded into HA-PBLG-LA CLNPs, and then injected into mice bearing human MCF-7 breast tumor (tumor size: ~100 mm^3) via tail vein. Human breast tumor xenograft model was established by subcutaneous inoculation of 1×10^7 MCF-7 cells in 50 μL PBS media into the hind flank of each mouse. The fluorescent scans were carried out at different time points of 2, 6, 10, 12 and 48 h following *i.v.* injection using the Maestro *in vivo* fluorescence imaging system (CRi Inc.).

Biodistribution of DOX-CLNPs was investigated using *ex vivo* fluorescence imaging based on the fluorescent nature of DOX. A single dose of DOX-CLNPs or DOX-LPs in 200 μL PB was administrated intravenously via the tail vein at a dosage of 10 mg DOX equiv./kg. After 6 h, MCF-7 tumor-bearing mice were sacrificed. The tumor block and several major organs including heart, liver, spleen, lung, and kidney were collected, washed, and dried. Fluorescence images were captured with the Maestro *in vivo* fluorescence imaging system (CRi Inc.). To quantify the amount of DOX delivered to the tumor and different organs, tumor-bearing mice following 6 h *i.v.* injection with DOX-CLNPs or DOX-LPs (10 mg DOX equiv./kg) were sacrificed. The tumor block and major organs (heart, liver, spleen, lung, and kidney) were collected, washed, weighed, then homogenized in 0.5 mL of 1% Triton X-100 with a Superfine Homogenizer (F6/10, Fluko). To the above tissue lysates, 0.9 mL of extraction solution of DMF containing 20 mM DTT was added. The samples were incubated overnight, and then centrifuged at 23 krpm for 30 min. The amount of DOX was quantified by fluorescence measurement.

2.12. In vivo antitumor efficacy

In vivo antitumor efficacy was examined in MCF-7 tumor-bearing mice. When tumors grew up to about 100 mm^3 in volume, DOX-CLNPs or DOX-LPs at a dosage of 7.5 mg DOX equiv./kg were intravenously administered every three days for four times. PBS was used as a blank control. The tumor sizes were measured by calipers every three days and volume was calculated according to the formula: $V = 0.5 \times L \times W \times H$, wherein L is the tumor dimension at the longest point, W is the tumor dimension at the widest point, and H is the tumor dimension at the highest point. Relative tumor volumes were calculated as V/V_0 (V_0 is the tumor volume at the start of treatment, and V is the tumor volume at any given day). Mice were weighed with the relative body weights compared to their initial weights. Mice in each group were considered to be dead either when the tumor volume increased to 1500 mm^3, or when the mice died during treatment. Maximum Tolerated Dosage (MTD) studies were evaluated in nude mice through a single intravenous injection of DOX-CLNPs (60 and 100 DOX equiv./kg) or DOX-LPs (10 and 20 mg DOX equiv./kg). Mice were weighed for 12 days with the relative body weights compared to their initial weights. The MTD was defined as the highest dose of DOX that does not cause over 15% body weight loss, unacceptable toxicity like death or other remarkable changes in the general appearance of the mice within the experiment period [35,36].

2.13. Histological analysis

At the end of the treatment, one mouse of each group was sacrificed, and the tumor, liver, heart and kidney were excised. The tissues were fixed with 4% paraformaldehyde solution and embedded in paraffin. The sliced organ tissues (thickness: 4 mm) mounted on the glass slides were stained by hematoxylin and eosin (H&E) and observed by a digital microscope (Leica QWin).

3. Results and discussion

3.1. Synthesis of HA-PBLG-LA conjugates

HA-PBLG-LA was readily synthesized by the ring-opening polymerization of BLG-NCA using LA-NH_2 as an initiator followed by conjugating to HA via carbodiimide chemistry (Scheme 2). ^{1}H NMR spectrum of LA-PBLG showed characteristic signals of PBLG (δ 7.17, 5.12, 4.60, 2.38, 2.10–1.89) and LA-NH_2 moieties (δ 4.36, 3.44, 3.26, 2.58, 1.60–1.20) (Fig. 1A). The degree of polymerization (DP) of LA-PBLG was determined by comparing the signal intensities of phenyl protons of PBLG (δ 7.17) and methylene of lipoic ring (δ 3.26), to be 7.9, 10.0 and 13.9 depending on molar feed ratios of BLG-NCA to LA-NH_2 (Table 1). The molecular weights of LA-PBLG determined by ^{1}H NMR were close to the design, indicating that PBLG had defined structure and controlled DP. MALDI-TOF mass spectrum further confirmed thus obtained LA-PBLG had a narrow molecular weight distribution with major peaks corresponding to m/z = 276.1 (LA-NH_2) + n × 219.1 (BLG) + 23.0 (Na^+) (Fig. S2). It should be mentioned that there exists also a minor mass distribution corresponding to m/z = 276.1 (LA-NH_2) + n × 219.1 (BLG) + 112.1 (pyroglutamate) + 23.0 (Na^+), which was atributed to formation of a cyclic end-group (pyroglutamate) as a result of backbiting reaction and elimination of benzyl alcohol [37]. The content of amino end group in PBLG was quantified by TNBSA assay to be 72.4%.

PBLG with a DP of 10 was employed to graft onto HA in the following study. ^{1}H NMR spectrum of HA-PBLG-LA displayed besides resonances owing to LA-PBLG moieties (δ 7.17, 5.02, 4.60, 2.94, 2.85, 2.63, 2.39, 2.14–1.89, 1.57–1.18) also signals attributable to HA backbone (δ 4.20, 3.93–3.72, 3.44–3.11) (Fig. 1B). The degree of substitution (DS), which is defined as the number of PBLG chain per 100 sugar residues of HA polymer, could be determined by comparing the integral of signals at δ 7.17 (phenyl protons in PBLG) and δ 4.20 (anomeric proton in HA). It is known that the CD44

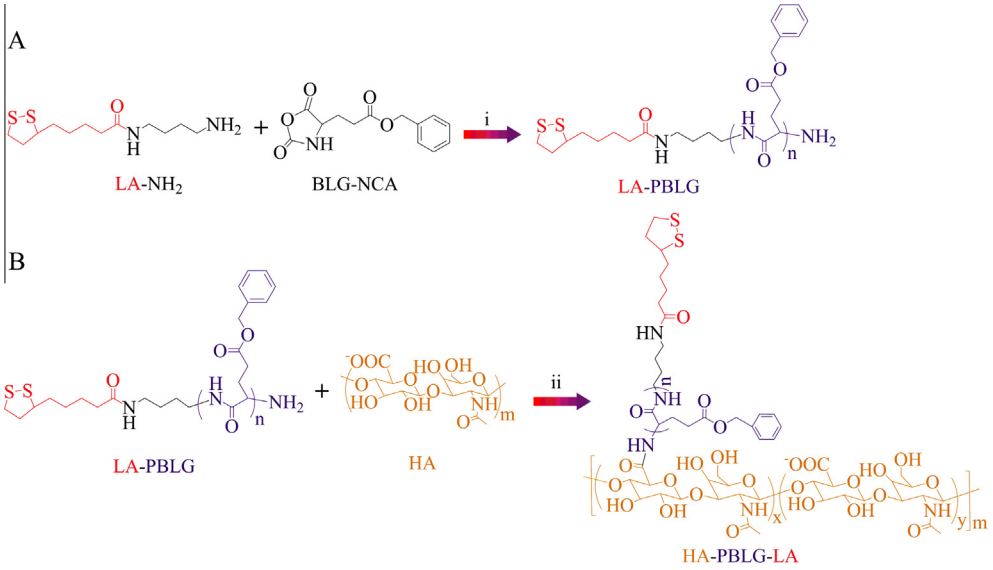

Scheme 2. Synthesis of HA-PBLG-LA conjugates. Conditions: (i) DMF, N_2, 30 °C, 3 d; (ii) EDC, NHS, 30 °C, DMSO/H_2O, 24 h.

Table 1
Synthesis of LA-PBLG polypeptides.

Entry	[M]/[I] (mol/mol)		M_n (kg/mol) ^{1}H NMR	Yield (%)
	Feed ratio	^{1}H NMR[a]		
1	8.0	7.9	2.0	76.4
2	10.0	10.0	2.5	80.4
3	14.0	13.9	3.3	82.5

[a] Calculated from ^{1}H NMR by comparing intensities of signals at δ 7.17 and 3.26, which were assignable to phenyl protons of PBLG and methylene protons of LA-NH_2, respectively.

receptor-binding property of HA is closely related to its carboxylic acid groups [38,39]. To retain a high tumor-targetability, HA-PBLG-LA conjugate with a low degree of substitution of 14 was prepared at a HA carboxyl group/LA-PBLG molar feed ratio of 2/1.

3.2. Formation and stability of crosslinked HA-PBLG-LA nanoparticles (CLNPs)

HA-PBLG-LA CLNPs were easily prepared through self-assembly of HA-PBLG-LA in water followed by auto-crosslinking in the presence of catalytic amount of dithiothreitol (DTT) as reported before [31,32,40]. DLS measurements revealed that CLNPs had an average diameter of 115 nm and a low polydispersity index (PDI) of 0.15 (Table 2). The stability tests revealed that HA-PBLG-LA CLNPs were robust against extensive dilution and 10% FBS (Fig. 2A). CLNPs swelled, however, to over 1000 nm in 12 h in the presence of 10 mM glutathione (GSH) under otherwise the same conditions (Fig. 2B), indicating that CLNPs are fast responsive to intracellular reductive environment. The largely increased size of CLNPs following treatment with 10 mM GSH is mainly due to increased hydrophilicity of nanoparticle core as disulfide crosslinks are transformed into dihydrolipoyl groups. Therefore, HA-PBLG-LA CLNPs while possess superior colloidal stability under physiological conditions are prone to rapid decrosslinking under a reductive condition mimicking that of the cytoplasm and cell nucleus.

Table 2
Characteristics of HA-PBLG-LA NCLNPs and CLNPs.

	Size[a] (nm)	PDI[a]	Zeta[b] (mV)	CMC[c] (mg/L)
NCLNPs	124	0.15	−20.4	9.2
CLNPs	115	0.12	−19.2	–

[a] Determined by DLS analysis using Zetasizer Nano-ZS (Malvern Instruments) at 25 °C in water.
[b] Measured using Zetasizer Nano-ZS (Malvern Instruments) equipped with a standard capillary electrophoresis cell at 25 °C in water.
[c] Determined using pyrene as a fluorescence probe.

3.3. Loading and reduction-triggered release of DOX

The loading of doxorubicin (DOX), a potent hydrophobic anticancer drug, was performed at a polymer concentration of 5 mg/mL and DOX feeding ratios of 20–40 wt.%. Notably, CLNPs exhibited a remarkably high drug loading content (DLC) of 25.8 wt.% and drug loading efficiency (DLE) of over 81.1%, in which both DLE and DLC increased with increasing DOX feed ratios (Table 3). DLS measurements showed that DOX-loaded CLNPs (DOX-CLNPs) had small sizes of 72–80 nm (Fig. 2C), which were smaller than blank CLNPs (115 nm) as well as clinically used DOX-LPs (~100 nm) [41]. In comparison, crosslinked HA-LA nanoparticles without PBLG block had much larger sizes (154–225 nm) and lower drug loading levels (less than 15.1%) [16]. The enhanced drug loading for CLNPs is likely due to the existence of π-π stacking interactions between DOX and the benzene groups in PBLG. Several groups have reported that π-π stacking can significantly enhance loading of drugs including DOX, paclitaxel and docetaxel into polymeric micelles with aromatic groups in the core [42–44]. TEM micrograph confirmed that DOX-CLNPs had small particle size and a spherical morphology (Fig. 2C). This small size is desired for nanomedicines to achieve enhanced tumor penetration and treatment effects [45,46]. The *in vitro* release studies showed that DOX release while largely inhibited under physiological conditions (pH 7.4, 37 °C) was significantly enhanced in the presence of 10 mM GSH (17.7% versus 91.5% release in 30 h) (Fig. 2D). It is interesting to note that DOX-CLNPs had less drug release under physiological conditions than reported HA-LA nanoparticles (24.2% release in 22 h) [16], signifying the important role of PBLG block in inhibiting drug leakage from CLNPs. Hence, DOX-CLNPs not only have a high drug loading capacity and a small size but also have a potential to solve the *in vivo* stability and drug release dilemma that persists as a long challenge for targeted nanotherapeutics [47,48].

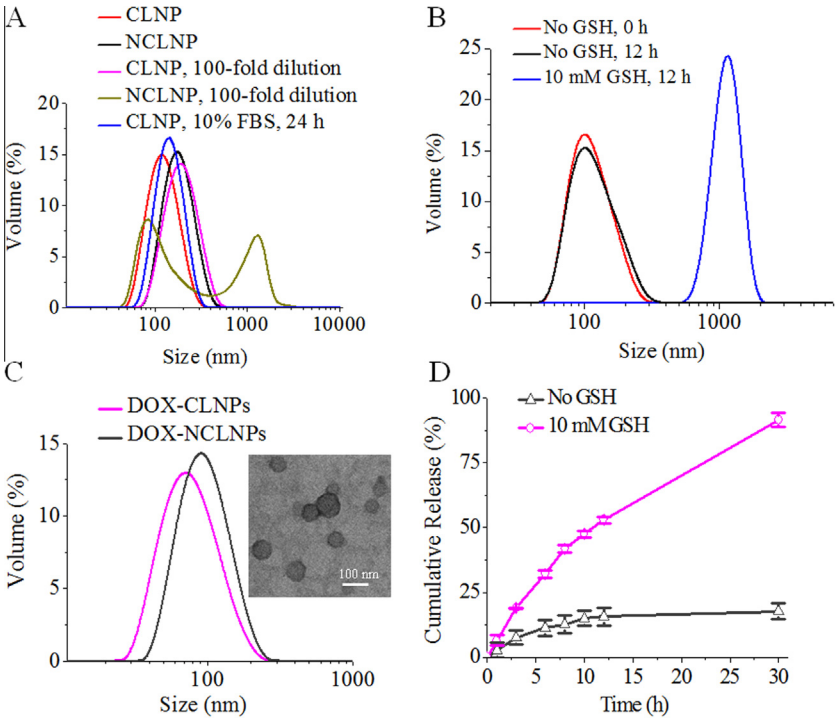

Fig. 2. Characteristics of crosslinked and noncrosslinked HA-PBLG-LA nanoparticles. (A) Size distribution and colloidal stability of HA-PBLG-LA CLNPs and NCLNPs measured by DLS; (B) change of size distribution profiles of HA-PBLG-LA CLNPs in response to 10 mM GSH in PB (pH 7.4, 10 mM) at 37 °C; (C) size distribution of DOX-CLNPs measured by DLS and TEM; (D) *in vitro* release of DOX in the presence or absence of 10 mM GSH from DOX-CLNPs. The drug release studies were performed at a concentration of 0.2 mg/mL. Data are presented as mean ± SD (n = 3).

Table 3
Characteristics of DOX-NCLNPs and DOX-CLNPs.

Entry	DOX feed ratio (wt.%)	NCLNPs		CLNPs		DLC (wt.%)	DLE (%)
		Size[a] (nm)	PDI[a]	Size[a] (nm)	PDI[a]		
1	20	89	0.16	72	0.14	14.0	81.1
2	30	93	0.17	74	0.15	20.1	83.9
3	40	99	0.23	80	0.23	25.8	87.1

[a] Determined by DLS analysis using Zetasizer Nano-ZS (Malvern Instruments) at 25 °C in water.

3.4. In vitro antitumor activity

To evaluate the cytotoxicity of blank CLNPs and antitumor activity of DOX-CLNPs, MTT assays were performed in CD44 receptor overexpressing MCF-7 breast cancer cells. The results showed that blank CLNPs were practically nontoxic at concentrations of 0.2–1.0 mg/mL (Fig. 3A), indicating that HA-PBLG-LA nanoparticles possess excellent biocompatibility. Notably, DOX-CLNPs induced obviously better antitumor effect than clinically used DOX-LPs (Fig. 3B). The half-maximal inhibitory concentration (IC_{50}) of DOX-CLNPs was determined to be 4.2 μg DOX equiv./mL (corresponds to a blank nanoparticle concentration of 16.7 μg/mL), which was though higher than that observed for free DOX fivefold lower than that of DOX-LPs (23 μg DOX equiv./mL). In contrast, DOX-CLNPs displayed a significantly lower antitumor activity to U87 cells (IC_{50} = 40 μg DOX equiv./mL) (Fig. 3B), confirming receptor-mediated uptake of DOX-CLNPs by MCF-7 cells.

To investigate the cellular uptake and intracellular drug release behaviors of DOX-CLNPs, we conducted flow cytometry and CLSM studies using MCF-7 cells. Interestingly, flow cytometry results showed that MCF-7 cells following 8 h incubation with DOX-CLNPs displayed more than 10-fold higher cellular DOX level than those with DOX-LPs (Fig. 3C). The pretreatment of MCF-7 cells with free HA prior to incubating with DOX-CLNPs resulted in markedly reduced cellular DOX level, further confirming that CLNPs were internalized by MCF-7 cells via a receptor-mediated mechanism [21]. CLSM images showed strong DOX fluorescence in the nuclei of MCF-7 cells following 12 h incubation with DOX-CLNPs, while weak DOX fluorescence was observed for DOX-LPs in MCF-7 cells as well as for DOX-CLNPs in MCF-7 cells pretreated with free HA (Fig. 3D). These results point out that DOX-CLNPs can actively target and release drug to CD44 overexpressing tumor cells. The high antitumor activity of DOX-CLNPs is likely due to a combination of efficient internalization by MCF-7 cells and rapid intracellular drug release. The pretreatment MCF-7 cells with free HA significantly reduced the anti-tumor activity of DOX-CLNPs, confirming that DOX-CLNPs were taken up by MCF-7 cells via a receptor-mediated mechanism.

3.5. In vivo pharmacokinetics and biodistribution

The *in vivo* pharmacokinetics of DOX-CLNPs was investigated by measuring the plasma DOX levels in mice following a single intravenous injection at a dosage of 10 mg DOX equiv./kg. Notably, DOX-CLNPs displayed a long circulation time with an elimination phase half-life of 4.9 h (Fig. 4A), approaching to that of DOX-LPs (8.1 h) which are well-known for its long circulation time *in vivo* [41]. Considerable amount of DOX was observed even at 24 h post injection. To visualize their *in vivo* tumor-targetability, DIR-loaded CLNPs were administered intravenously to nude mice bearing human breast MCF-7 tumor xenografts and monitored via a Maestro EX *in vivo* fluorescence imaging system (CRi, Inc.). Interestingly, significant DIR fluorescence was observed in the tumor at 2 h post injection and tumor DIR fluorescence intensity became stronger at 6–12 h and remained strong even at 48 h post injection

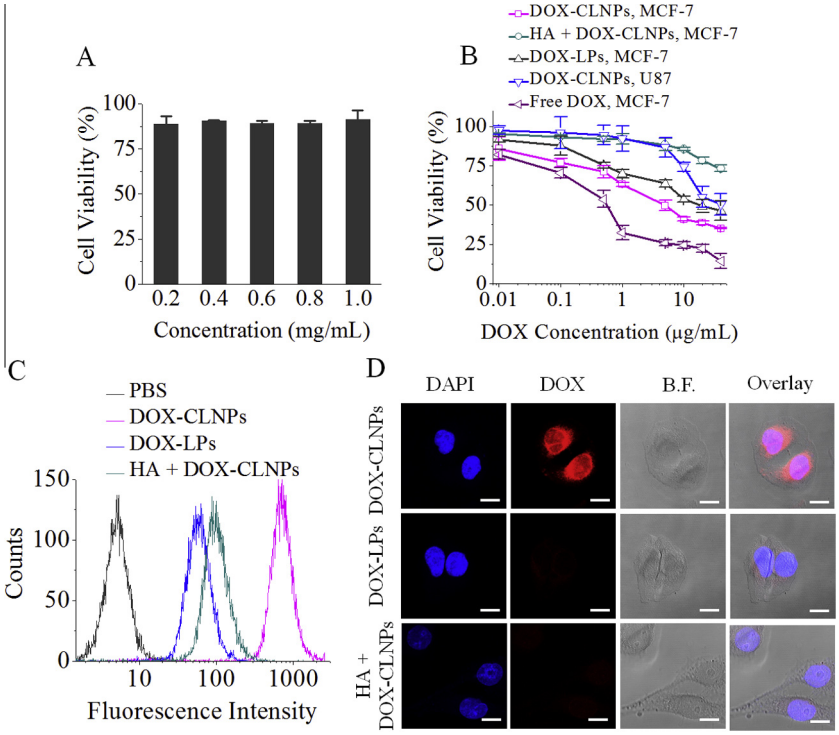

Fig. 3. Characteristics of DOX-CLNPs in MCF-7 cells. (A) Cytotoxicity of blank CLNPs determined by MTT assays in MCF-7 cells. The cells were incubated with CLNPs for 48 h. Data are presented as mean ± SD (n = 4); (B) antitumor activity of DOX-CLNPs and DOX-LPs in MCF-7 cells. The cells were treated with DOX-CLNPs for 4 h, the medium was removed and replenished with fresh culture medium, and the cells were incubated for another 48 h. The inhibition experiment was performed by pre-treating cells for 4 h with free HA (5 mg/mL) prior to incubation with DOX-CLNPs. Data are presented as mean ± SD (n = 4); (C) flow cytometry of MCF-7 cells following 8 h incubation with DOX-CLNPs and DOX-LPs (DOX dosage: 5.0 μg/mL). The competitive inhibition experiment was performed by pretreating cells with free HA (5 mg/mL) for 4 h before adding DOX-CLNPs; (D) CLSM images of MCF-7 cells incubated with DOX-CLNPs (DOX dosage: 10.0 μg/mL). The scale bars correspond to 20 μm in all the images.

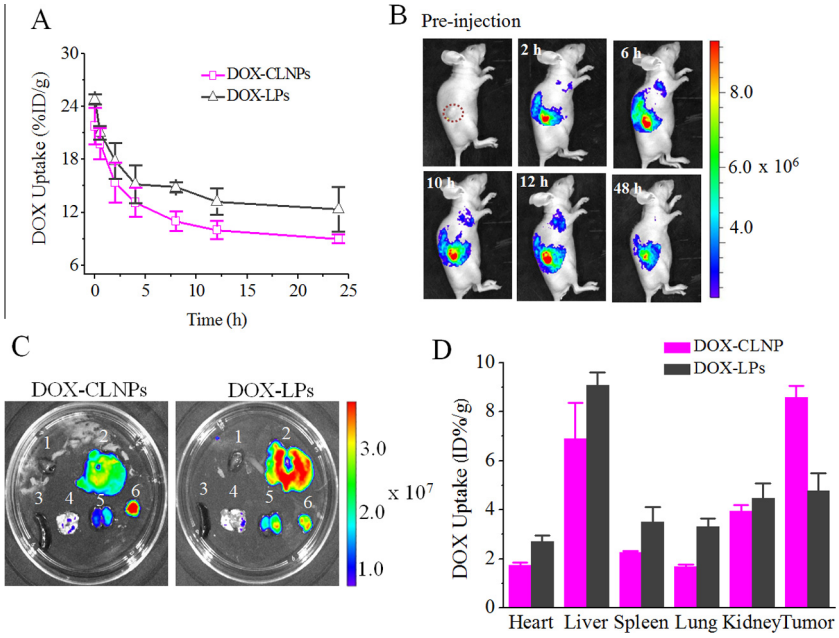

Fig. 4. *In vivo* pharmacokinetics and biodistribution. (A) *In vivo* pharmacokinetics of DOX-CLNPs and DOX-LPs in mice. DOX levels were determined by fluorescence spectroscopy. DOX uptake is expressed as injected dose per gram of tissue (% ID/g). Data are presented as mean ± SD (n = 3); (B) *in vivo* fluorescence images of MCF-7 human breast tumor bearing nude mice at different time points following injection of DIR-loaded CLNPs. The mouse autofluorescence was removed by spectral unmixing using the Maestro software; (C) DOX fluorescence images of tumors and major organs (1: heart, 2: liver, 3: spleen, 4: lung, 5: kidney, and 6: tumor) harvested from MCF-7 human breast tumor bearing nude mice following 6 h post intravenous injection of DOX-CLNPs and DOX-LPs, respectively; (D) quantification of DOX accumulated in different organs and tumors using fluorescence spectroscopy. DOX uptake is expressed as injected dose per gram of tissue (% ID/g). Data are presented as mean ± SD (n = 3).

(Fig. 4B), confirming high tumor accumulation and long retention of CLNPs *in vivo*.

To further examine their *in vivo* distribution, tumor and several major organs of MCF-7 tumor-bearing nude mice following 6 h *i.v.* injection of DOX-CLNPs or DOX-LPs were excised for *ex vivo* fluorescence imaging. Intriguingly, mice treated with DOX-CLNPs revealed intense DOX fluorescence in the tumor, which was significantly stronger than that in the major organs such as heart, liver, spleen, lung and kidney (Fig. 4C). In comparison, mice treated with DOX-LPs exhibited obviously weaker tumor DOX fluorescence and moreover strong DOX fluorescence was observed in the liver and kidney. As DOX fluorescence stems mainly from free DOX but not DOX-CLNPs [49], these results indicate that DOX-CLNPs can effectively target and release drug to human MCF-7 breast tumor xenografts *in vivo*. To quantify its *in vivo* biodistribution, DOX in tumor and major organs was extracted and measured using fluorometry. Notably, DOX-CLNPs demonstrated a strikingly high tumor DOX uptake of 8.6% of injected dose per gram of tissue (%ID/g), which was almost two times of that for DOX-LPs (Fig. 4D). It should be mentioned that nanotherapeutics have typically less than 5%ID/g accumulation in the tumor sites [50,51]. The high tumor DOX level achieved by DOX-CLNPs is likely due to a combination of small size, low drug leakage, long circulation time, and selective tumor homing. Importantly, DOX-CLNPs also reduced DOX accumulation in the healthy organs particularly heart, liver, spleen, and lung as compared to DOX-LPs, indicating that DOX-CLNPs can further reduce the systemic side effects including cardiomyopathy and congestive heart failure [52,53].

3.6. In vivo therapeutic efficacy

The therapeutic efficacy of DOX-CLNPs in MCF-7 human breast tumor-bearing nude mice was investigated and compared with DOX-LPs. The results showed that both DOX-CLNPs and DOX-LPs could effectively inhibit tumor growth at a dosage of 7.5 mg DOX equiv./kg (Fig. 5A). Importantly, DOX-CLNPs group exhibited no body weight loss (Fig. 5B), indicating that DOX-CLNPs have little systemic toxicity. On the contrary, DOX-LPs group displayed continuous body weight loss, serious hand-foot syndrome, and even death as from day 8. It is likely that the suppressed tumor growth observed for DOX-LPs is partly due to their systemic toxic effect. The Kaplan–Meier survival curves showed that DOX-CLNP group all survived within an experimental period of 52 d (Fig. 5C). In comparison, mice treated with DOX-LPs and PBS had median survival times of 13 d and 29 d, respectively. The short survival time observed for DOX-LPs mainly results from their pronounced side effects, while the short survival time for PBS treated group derives from the fast tumor growth. The histological analysis using H&E staining revealed that both DOX-CLNPs and DOX-LPs caused widespread tumor cell necrosis characterized by nuclei lysis (Fig. 6). In contrast to DOX-LPs that generated significant damage to liver with obscure boundary of hepatic cells, heart with disorganized cardiomyocyte structure, and kidney with inflammatory cell infiltration in renal interstitial, DOX-CLNPs resulted in little damage to the healthy organs. For clinical use, it is of critical importance for nanotherapeutics to possess a high therapeutic index. Here, the maximum-tolerated dose (MTD) was evaluated by a single *i.v.* administration of DOX-CLNPs and DOX-LPs in nude mice followed by body weight measurement and toxicity observation for 12 d. Remarkably, DOX-CLNPs were shown to cause little mice body weight loss even at a high dosage of 100 mg DOX equiv./kg (Fig. 5D), indicating that DOX-CLNPs have an MTD of over 100 mg DOX equiv./kg, which is higher than most of the reported DOX nanomedicines [54,55]. In contrast, DOX-LPs resulted in significant body weight loss and obvious hand-foot syndrome at 20 mg DOX equiv./kg. Hence, DOX-CLNPs have at least 5 times improvement of MTD over clinically used DOX-LPs, confirming that DOX-CLNPs have superior tolerability. The remarkably high MTD of DOX-CLNPs is likely due to their exceptional stability, selective tumor accumulation, and low uptake in major organs. The broad therapeutic window of DOX-CLNPs might allow effective treatment of various malignancies without causing dose-limiting side effects.

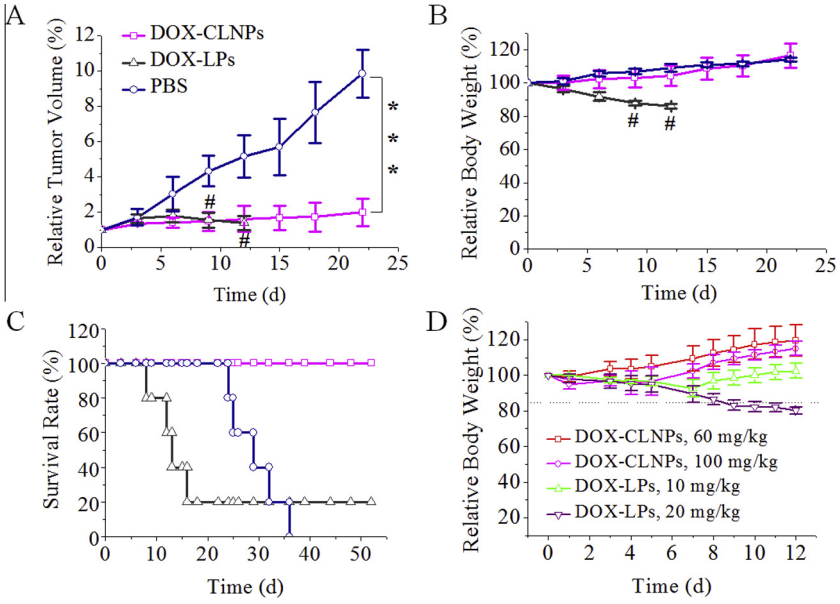

Fig. 5. *In vivo* antitumor performance of DOX-CLNPs in MCF-7 human breast tumor-bearing nude mice. (A) Tumor volume changes of mice treated with DOX-CLNPs, DOX-LPs and PBS, respectively. The drug was given on days 0, 3, 6, and 9 (dosage: 7.5 mg DOX equiv./kg in 0.2 mL PBS). Data are presented as mean ± SD (n = 6). "#" denotes one mouse died during treatment; (B) bodyweight changes of mice in different treatment groups within 22 d. Data are presented as mean ± SD (n = 6); (C) survival rates of mice in different treatment groups within 52 d; (D) maximum-tolerated dose (MTD) evaluated by a single *i.v.* administration of DOX-CLNPs and DOX-LPs in nude mice followed by body weight measurement for 12 d. Data are presented as mean ± SD (n = 6).

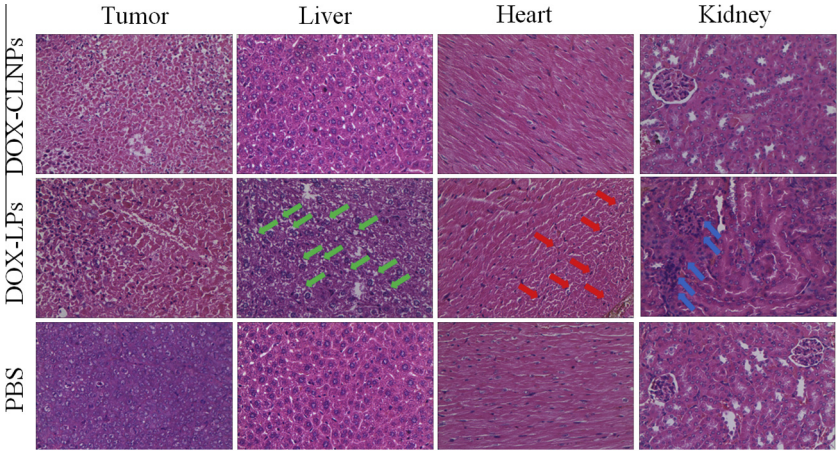

Fig. 6. H&E staining assays of tumor, live, heart and kidney sections excised from tumor-bearing mice following 15 d treatment with DOX-CLNP, DOX-LPs, and PBS. The images were obtained by a Leica microscope at magnification (400×). The arrows indicate destroyed cell morphology and vacuoles in cytoplasm in liver, disorganized cell structure in heart, and inflammatory cell infiltration in renal interstitial, respectively.

4. Conclusions

We have demonstrated for the first time that doxorubicin-loaded multifunctional nanoparticles based on hyaluronic acid-g-poly(γ-benzyl-L-glutamate)-lipoic acid conjugates, which are derived from natural endogenous materials, possess a high drug loading, superior stability, triggered cytoplasmic drug release, high tolerability and therapeutic index, and enhanced tumor accumulation and selectivity toward CD44-overexpressing tumors *in vivo*. The therapeutic studies clearly show that these robust, fast bioresponsive and highly specific nanotherapeutics cause little side effects and can effectively suppress tumor growth and drastically improve the survival rate of CD44-posive MCF-7 human breast tumor-bearing nude mice, greatly outperforming the clinically used pegylated polymersomal doxorubicin. It should further be noted that unlike previously reported multifunctional nanomedicines, the present nanotherapeutics primarily based on natural endogenous materials are simple and straightforward to fabricate. This proof-of-concept study highlights that with rational design, we are likely able to develop simple and multifunctional anticancer nanotherapeutics to achieve better cancer chemotherapy with reduced adverse effects.

Acknowledgments

This work was supported by the National Natural Science Foundation of China (NSFC 51273137, 51473110 and 51403147) and the National Science Fund for Distinguished Young Scholars (NSFC 51225302). Z.Z. thanks the Friedrich Wilhelm Bessel Research Award from the Alexander von Humboldt Foundation.

Appendix A. Supplementary data

Supplementary data associated with this article can be found, in the online version, at http://dx.doi.org/10.1016/j.actbio.2016.08.048.

References

[1] K. Bourzac, Nanotechnology carrying drugs, Nature 491 (2012) S58–S60.
[2] R. Cheng, F. Meng, C. Deng, Z. Zhong, Bioresponsive polymeric nanotherapeutics for targeted cancer chemotherapy, Nano Today 10 (2015) 656–670.
[3] Y. Min, J.M. Caster, M.J. Eblan, A.Z. Wang, Clinical translation of nanomedicine, Chem. Rev. 115 (2015) 11147–11190.
[4] H. Cabral, K. Kataoka, Progress of drug-loaded polymeric micelles into clinical studies, J. Control. Release 190 (2014) 465–476.
[5] A. Wicki, D. Witzigmann, V. Balasubramanian, J. Huwyler, Nanomedicine in cancer therapy: challenges, opportunities, and clinical applications, J. Control. Release 200 (2015) 138–157.
[6] A.C. Anselmo, S. Mitragotri, An overview of clinical and commercial impact of drug delivery systems, J. Control. Release 190 (2014) 15–28.
[7] V.P. Chauhan, R.K. Jain, Strategies for advancing cancer nanomedicine, Nat. Mater. 12 (2013) 958–962.
[8] T. Lammers, F. Kiessling, W.E. Hennink, G. Storm, Drug targeting to tumors: principles, pitfalls and (pre-) clinical progress, J. Control. Release 161 (2012) 175–187.
[9] C. Deng, Y. Jiang, R. Cheng, F. Meng, Z. Zhong, Biodegradable polymeric micelles for targeted and controlled anticancer drug delivery: promises, progress and prospects, Nano Today 7 (2012) 467–480.
[10] V.P. Torchilin, Multifunctional, stimuli-sensitive nanoparticulate systems for drug delivery, Nat. Rev. Drug Discov. 13 (2014) 813–827.
[11] N. Kamaly, Z. Xiao, P.M. Valencia, A.F. Radovic-Moreno, O.C. Farokhzad, Targeted polymeric therapeutic nanoparticles: design, development and clinical translation, Chem. Soc. Rev. 41 (2012) 2971–3010.
[12] H. Yu, Z. Cui, P. Yu, C. Guo, B. Feng, T. Jiang, S. Wang, Q. Yin, D. Zhong, X. Yang, Z. Zhang, Y. Li, PH- and NIR light-responsive micelles with hyperthermia-triggered tumor penetration and cytoplasm drug release to reverse doxorubicin resistance in breast cancer, Adv. Funct. Mater. 25 (2015) 2489–2500.
[13] D. Ling, W. Park, S.-J. Park, Y. Lu, K.S. Kim, M.J. Hackett, B.H. Kim, H. Yim, Y.S. Jeon, K. Na, T. Hyeon, Multifunctional tumor pH-sensitive self-assembled nanoparticles for bimodal imaging and treatment of resistant heterogeneous tumors, J. Am. Chem. Soc. 136 (2014) 5647–5655.
[14] L. Chen, Z. Zhang, X. Chen, X. Yao, C. He, X. Chen, Fabrication of modular multifunctional delivery for antitumor drugs based on host-guest recognition, Acta Biomater. 18 (2015) 168–175.
[15] K. Raemdonck, S.C. De Smedt, Lessons in simplicity that should shape the future of drug delivery, Nat. Biotechnol. 33 (2015) 1026–1027.
[16] Y. Zhong, J. Zhang, R. Cheng, C. Deng, F. Meng, F. Xie, Z. Zhong, Reversibly crosslinked hyaluronic acid nanoparticles for active targeting and intelligent delivery of doxorubicin to drug resistant CD44+ human breast tumor xenografts, J. Control. Release 205 (2015) 144–154.
[17] C.H. Evans, V.B. Kraus, L.A. Setton, Progress in intra-articular therapy, Nat. Rev. Rheumatol. 10 (2014) 11–22.
[18] H. Lee, M.-Y. Lee, S.H. Bhang, B.-S. Kim, Y.S. Kim, J.H. Ju, K.S. Kim, S.K. Hahn, Hyaluronate-gold nanoparticle/tocilizumab complex for the treatment of rheumatoid arthritis, ACS Nano 8 (2014) 4790–4798.
[19] E.J. Oh, K. Park, K.S. Kim, J. Kim, J.-A. Yang, J.-H. Kong, M.Y. Lee, A.S. Hoffman, S. K. Hahn, Target specific and long-acting delivery of protein, peptide, and nucleotide therapeutics using hyaluronic acid derivatives, J. Control. Release 141 (2010) 2–12.
[20] K.K. Upadhyay, A.N. Bhatt, A.K. Mishra, B.S. Dwarakanath, S. Jain, C. Schatz, J.-F. Le Meins, A. Farooque, G. Chandraiah, A.K. Jain, A. Misra, S. Lecommandoux, The intracellular drug delivery and anti tumor activity of doxorubicin loaded poly(gamma-benzyl L-glutamate)-b-hyaluronan polymersomes, Biomaterials 31 (2010) 2882–2892.
[21] S. Arpicco, P. Milla, B. Stella, F. Dosio, Hyaluronic acid conjugates as vectors for the active targeting of drugs, genes and nanocomposites in cancer treatment, Molecules 19 (2014) 3193–3230.
[22] C. Schatz, S. Louguet, J.-F. Le Meins, S. Lecommandoux, Polysaccharide-block-polypeptide copolymer vesicles: towards synthetic viral capsids, Angew. Chem. Int. Ed. 48 (2009) 2572–2575.

[23] H. Tian, W. Xiong, J. Wei, Y. Wang, X. Chen, X. Jing, Q. Zhu, Gene transfection of hyperbranched PEI grafted by hydrophobic amino acid segment PBLG, Biomaterials 28 (2007) 2899–2907.
[24] Y. Matsumura, K. Kataoka, Preclinical and clinical studies of anticancer agent-incorporating polymer micelles, Cancer Sci. 100 (2009) 572–579.
[25] C. Li, S. Wallace, Polymer-drug conjugates: recent development in clinical oncology, Adv. Drug Deliv. Rev. 60 (2008) 886–898.
[26] C. Deng, J. Wu, R. Cheng, F. Meng, H.-A. Klok, Z. Zhong, Functional polypeptide and hybrid materials: precision synthesis via alpha-amino acid N-carboxyanhydride polymerization and emerging biomedical applications, Prog. Polym. Sci. 39 (2014) 330–364.
[27] K.P. Shay, R.F. Moreau, E.J. Smith, A.R. Smith, T.M. Hagen, Alpha-lipoic acid as a dietary supplement: molecular mechanisms and therapeutic potential, Biochim. Biophys. Acta Gen. Subj. 1790 (2009) 1149–1160.
[28] A. Maczurek, K. Hager, M. Kenklies, M. Sharman, R. Martins, J. Engel, D.A. Carlson, G. Muench, Lipoic acid as an anti-inflammatory and neuroprotective treatment for alzheimer's disease, Adv. Drug Deliv. Rev. 60 (2008) 1463–1470.
[29] P. Chen, M. Qiu, C. Deng, F. Meng, J. Zhang, R. Cheng, Z. Zhong, PH-responsive chimaeric pepsomes based on asymmetric poly(ethylene glycol)-b-poly(L-leucine)-b-poly(L-glutamic acid) triblock copolymer for efficient loading and active intracellular delivery of doxorubicin hydrochloride, Biomacromolecules 16 (2015) 1322–1330.
[30] A.J. Williams, V.K. Gupta, Self-assembly of a rodlike polypeptide on solid surfaces: role of solvent, molecular weight, and time of assembly, J. Phys. Chem. B 105 (2001) 5223–5230.
[31] Y.-L. Li, L. Zhu, Z. Liu, R. Cheng, F. Meng, J.-H. Cui, S.-J. Ji, Z. Zhong, Reversibly stabilized multifunctional dextran nanoparticles efficiently deliver doxorubicin into the nuclei of cancer cells, Angew. Chem. Int. Ed. 48 (2009) 9914–9918.
[32] L. Wu, Y. Zou, C. Deng, R. Cheng, F. Meng, Z. Zhong, Intracellular release of doxorubicin from core-crosslinked polypeptide micelles triggered by both pH and reduction conditions, Biomaterials 34 (2013) 5262–5272.
[33] H.J. Cho, H.Y. Yoon, H. Koo, S.H. Ko, J.S. Shim, J.H. Lee, K. Kim, I.C. Kwon, D.D. Kim, Self-assembled nanoparticles based on hyaluronic acid-ceramide (HA-CE) and pluronic (®) for tumor-targeted delivery of docetaxel, Biomaterials 32 (2011) 7181–7190.
[34] K.K. Upadhyay, A.N. Bhatt, A.K. Mishra, B.S. Dwarakanath, S. Jain, C. Schatz, J.F. Le Meins, A. Farooque, G. Chandraiah, A.K. Jain, A. Misra, S. Lecommandoux, The intracellular drug delivery and anti tumor activity of doxorubicin loaded poly(gamma-benzyl L-glutamate)-b-hyaluronan polymersomes, Biomaterials 31 (2010) 2882–2892.
[35] W. Xu, J. Ding, C. Xiao, L. Li, X. Zhuang, X. Chen, Versatile preparation of intracellular-acidity-sensitive oxime-linked polysaccharide-doxorubicin conjugate for malignancy therapeutic, Biomaterials 54 (2015) 72–86.
[36] P. Zhang, Y. Huang, H. Liu, R.T. Marquez, J. Lu, W. Zhao, X. Zhang, X. Gao, J. Li, R. Venkataramanan, L. Xu, S. Li, A PEG-Fmoc conjugate as a nanocarrier for paclitaxel, Biomaterials 35 (2014) 7146–7156.
[37] R.J.I. Knoop, G.J.M. Habraken, N. Gogibus, S. Steig, H. Menzel, C.E. Koning, A. Heise, Synthesis of poly(benzyl glutamate-b-styrene) rod-coil block copolymers by dual initiation in one pot, J. Polym. Sci. Part A Polym. Chem. 46 (2008) 3068–3077.
[38] N.V. Rao, H.Y. Yoon, H.S. Han, H. Ko, S. Son, M. Lee, H. Lee, D.-G. Jo, Y.M. Kang, J. H. Park, Recent developments in hyaluronic acid-based nanomedicine for targeted cancer treatment, Expert Opin. Drug Deliv. 13 (2016) 239–252.
[39] J.-A. Yang, W.H. Kong, D.K. Sung, H. Kim, T.H. Kim, K.C. Lee, S.K. Hahn, Hyaluronic acid-tumor necrosis factor-related apoptosis-inducing ligand conjugate for targeted treatment of liver fibrosis, Acta Biomater. 12 (2015) 174–182.
[40] S. Yu, J. Ding, C. He, Y. Cao, W. Xu, X. Chen, Disulfide cross-linked polyurethane micelles as a reduction-triggered drug delivery system for cancer therapy, Adv. Healthc. Mater. 3 (2014) 752–760.
[41] Y. Barenholz, Doxil (®) – the first FDA-approved nano-drug: lessons learned, J. Control. Release 160 (2012) 117–134.
[42] Y. Shi, R. van der Meel, B. Theek, E.O. Blenke, E.H.E. Pieters, M.H.A.M. Fens, J. Ehling, R.M. Schiffelers, G. Storm, C.F. van Nostrum, T. Lammers, W.E. Hennink, Complete regression of xenograft tumors upon targeted delivery of paclitaxel via pi-pi stacking stabilized polymeric micelles, ACS Nano 9 (2015) 3740–3752.
[43] M.G. Carstens, J.J.L. Bevernage, C.F. van Nostrum, M.J. van Steenbergen, F.M. Flesch, R. Verrijk, L.G.J. de Leede, D.J.A. Crommelin, W.E. Hennink, Small oligomeric micelles based on end group modified mPEG-oligocaprolactone with monodisperse hydrophobic blocks, Macromolecules 40 (2007) 116–122.
[44] Y. Liang, X. Deng, L. Zhang, X. Peng, W. Gao, J. Cao, Z. Gu, B. He, Terminal modification of polymeric micelles with pi-conjugated moieties for efficient anticancer drug delivery, Biomaterials 71 (2015) 1–10.
[45] H. Cabral, Y. Matsumoto, K. Mizuno, Q. Chen, M. Murakami, M. Kimura, Y. Terada, M.R. Kano, K. Miyazono, M. Uesaka, N. Nishiyama, K. Kataoka, Accumulation of sub-100 nm polymeric micelles in poorly permeable tumours depends on size, Nat. Nanotechnol. 6 (2011) 815–823.
[46] J. Wang, W. Mao, L.L. Lock, J. Tang, M. Sui, W. Sun, H. Cui, D. Xu, Y. Shen, The role of micelle size in tumor accumulation, penetration, and treatment, ACS Nano 9 (2015) 7195–7206.
[47] H. Wei, R.-X. Zhuo, X.-Z. Zhang, Design and development of polymeric micelles with cleavable links for intracellular drug delivery, Prog. Polym. Sci. 38 (2013) 503–535.
[48] J. Li, X. Yu, Y. Wang, Y. Yuan, H. Xiao, D. Cheng, X. Shuai, A reduction and pH dual-sensitive polymeric vector for long-circulating and tumor-targeted siRNA delivery, Adv. Mater. 26 (2014) 8217–8224.
[49] Y. Zhu, J. Zhang, F. Meng, C. Deng, R. Cheng, J. Feijen, Z. Zhong, CRGD-functionalized reduction-sensitive shell-sheddable biodegradable micelles mediate enhanced doxorubicin delivery to human glioma xenografts in vivo, J. Control. Release 233 (2016) 29–38.
[50] C.J. Rijcken, C.J. Snel, R.M. Schiffelers, C.F. van Nostrum, W.E. Hennink, Hydrolysable core-crosslinked thermosensitive polymeric micelles: synthesis, characterisation and in vivo studies, Biomaterials 28 (2007) 5581–5593.
[51] R. Tong, H.H. Chiang, D.S. Kohane, Photoswitchable nanoparticles for in vivo cancer chemotherapy, PNAS 110 (2013) 19048–19053.
[52] Y. Octavia, C.G. Tocchetti, K.L. Gabrielson, S. Janssens, H.J. Crijns, A.L. Moens, Doxorubicin-induced cardiomyopathy: from molecular mechanisms to therapeutic strategies, J. Mol. Cell. Cardiol. 52 (2012) 1213–1225.
[53] G. Takemura, H. Fujiwara, Doxorubicin-induced cardiomyopathy from the cardiotoxic mechanisms to management, Prog. Cardiovasc. Dis. 49 (2007) 330–352.
[54] S. Lv, M. Li, Z. Tang, W. Song, H. Sun, H. Liu, X. Chen, Doxorubicin-loaded amphiphilic polypeptide-based nanoparticles as an efficient drug delivery system for cancer therapy, Acta Biomater. 9 (2013) 9330–9342.
[55] J. Lu, W. Zhao, H. Liu, R. Marquez, Y. Huang, Y. Zhang, J. Li, W. Xie, R. Venkataramanan, L. Xu, S. Li, An improved D-alpha-tocopherol-based nanocarrier for targeted delivery of doxorubicin with reversal of multidrug resistance, J. Control. Release 196 (2014) 272–286.